Crooked tail (*Cd*) model of human folate-responsive neural tube defects is mutated in Wnt coreceptor lipoprotein receptor-related protein 6

Michelle Carter*†, Xu Chen*†, Bozena Slowinska*, Sharon Minnerath‡§, Sara Glickstein*, Lei Shi¶, Fabien Campagne¶‖, Harel Weinstein¶‖, and M. Elizabeth Ross*,**

Departments of *Neurology and Neuroscience and ‖Physiology and Biophysics and ¶Institute for Computational Biomedicine, Weill Medical College of Cornell University, New York, NY 10021; and ‡Department of Neurology, University of Minnesota Medical School, Minneapolis, MN 55455

Edited by Kathryn V. Anderson, Sloan–Kettering Institute, New York, NY, and approved July 29, 2005 (received for review March 9, 2005)

A cranial neural tube defect in *Crooked tail* (*Cd*) mice is prevented with prenatal dietary folic acid *Cd* positional cloning reveals a missense mutation of a highly conserved amino acid in the low density lipoprotein receptor-related protein 6 (*Lrp6*), a coreceptor required for Wnt canonical signaling. Molecular modeling predicts that $Lrp6^{Cd}$ alters a hinge region of the second YWTD β-propeller domain. Mutant LRP6 binds to Wnt and Dickkopf1 (Dkk1) but not Mesd1, and Dkk1 cannot antagonize Wnt in *Cd*/*Cd* cells, resulting in hyperactivity. NIH 3T3 cells transfected with a mutant Lrp6 plasmid resist Dkk1 antagonism much like *Cd*/+ cells, confirming the significance of the mutation. The *Lrp6* mutation in *Cd* mice provides evidence for a functional connection between Wnt signaling and folate rescue of neural tube defects.

folic acid | Wnt signaling

Neural tube defects (NTD), including anencephaly and spina bifida, affect 0.5–1 per 1,000 live births worldwide (1). They can occur alone or associated with other anomalies that include limbs, craniofacial structures, heart, or kidney. Genetics contribute to NTD, but associations between variant genes and NTD phenotypes are difficult to establish because of gene interactions and incomplete penetrance, producing only a 1-in-10 recurrence risk in families with two affected siblings (2). Despite this genetic complexity, the vitamin folic acid has been found in multiple clinical studies to reduce the risk of NTD by as much as 50–70%, even in the absence of nutritional deficiency (3, 4). Many studies of folate levels and transport found no robust connection between NTD and the folic acid metabolic pathway that could explain folate's broad benefit. Understanding its action will require comparison at the molecular, cellular, and systems levels of animal models whose NTD are prevented by folate and those that are resistant to the vitamin.

The NTD in *Crooked tail* (*Cd*) mice is ameliorated by dietary folate in a manner that closely parallels clinical studies, making it an excellent model of folate-responsive NTD in humans (5). Heterozygous *Cd*/+ mice display a crooked tail whereas *Cd*/*Cd* animals maintained on a 4 mg of folate/kg of chow prenatal diet reveal phenotypes that include early postimplantation lethality (20–30% of homozygotes) and exencephaly (20–30%). *Cd*/*Cd* fetuses that close the cranial neural tube are viable but are runted (≈25% of *Cd*/*Cd* mice), with more severe malformations of various tail and lumbar vertebrae compared with *Cd*/+ siblings.

Here, a missense mutation in *Cd* replaces a single highly conserved amino acid in the low-density lipoprotein (LDL) receptor-related protein, LRP6. LRP6 (Arrow in *Drosophila*) is a LDL coreceptor for wingless (Wnt), and either LRP6 or LRP5 is required for Wnt signaling via the frizzled (Fz) receptor-β catenin pathway (6–8). Previously, complete inactivation of *Lrp6* by gene insertion was shown to produce exencephaly, spina bifida, absent tail, and limb deformities (7) whereas a hypomorphic point mutation in *Lrp6* produces osteoporosis and spina bifida (9). The *Cd* mutation does not inactivate canonical Wnt signaling but instead ablates the ability of Dickkopf1 (Dkk1) to inhibit Wnt, producing a net hyperactive allele. NTD in mice have now been associated with loss of *Lrp6* (7), *disheveled 2 (Dvl2)*, and *Dvl1/2* double nulls (10), *Axin* (11), and with missense mutations in *Lrp6* causing hypo- or hyperactivity (ref. 9 and this report). Thus, genetic variants in Wnt signaling pathways can result in NTD. Identification of Lrp6 mutation in *Crooked tail* represents an indication that Wnt pathway genes can be involved in folate-responsive NTD.

Methods

Colony Maintenance. *Cd*/+ were mated with DBA/2J mice (The Jackson Laboratory). Crooked-tailed F_1 offspring were then mated to A/J mice (The Jackson Laboratory) to produce N_2 offspring. At postnatal day 18, N_2 pups were phenotyped for a crooked tail. Embryos and live offspring were phenotyped by visual inspection, and, in some instances, skeletal preparations were made by using standard procedures (12). For complementation studies, $Lrp6^{+/-}$ mice were crossed with $Cd^{+/-}$, and the *Cd* and $Lrp6^{-}$ alleles were genotyped as described (5, 7).

Genotyping. A panel of 23 polymorphic markers (13) on distal chromosome 6 (Research Genetics, Huntsville, AL) were used to haplotype 1,043 crooked-tailed N_2 mice by using PCR conditions as detailed in the report of the first 221 N_2 animals (5). One SNP identified in exon 4 of *Rai3* was used to distinguish *Cd* from DBA among the 14 samples showing recombination with *Cd* between D6Mit111 and D6Mit301.

Genetic Map. Gene order and recombination distances were determined from genotyping results for 1,043 N_2 offspring by using the MAP MANAGER program (14).

Identification and Sequencing of Candidate Genes. The mouse genome (Ensembl Genome Browser) was searched for candidate genes between markers D6Mit111 and D6Mit301. The mouse genome database indicated that 18 known or predicted genes were in the region (15, 16). Sequencing and PCR primers for all 72 exons from 14 genes were designed, and sequences from

This paper was submitted directly (Track II) to the PNAS office.

Abbreviations: NTD, neural tube defect; *Cd, Crooked tail*; LDL, low-density lipoprotein; LDLR, LDL receptor; LRP6, lipoprotein receptor-related protein 6; *Fz, frizzled*; MEF, mouse embryonic fibroblasts; Dkk1, Dickkopf1; co-IP, coimmunoprecipitation; CM, conditioned media; E*n*, embryonic day *n*.

†M.C. and X.C. contributed equally to this work.

§Present address: Department of Laboratory Medicine and Pathology, University of Minnesota Medical School, Minneapolis, MN 55455.

**To whom correspondence should be addressed at: Laboratory of Neurogenetics and Development, Weill Medical College of Cornell University, New York, NY 10021. E-mail: mer2005@med.cornell.edu.

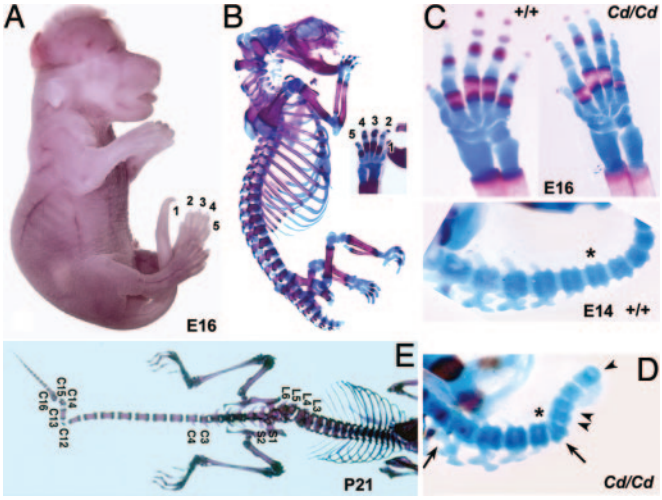

Fig. 1. *Cd* mice display cranial but not spinal NTD. (*A*) An E16 *Cd*/*Cd* exencephalic embryo has normal limbs and no tail truncation. (*B*) The same E16 embryo after skeletal staining with alizarin red (bone) and alcian blue (cartilage) (right forepaw shown in *Inset*). Tail vertebrae are unstained because cutaneous tissue was not dissected away. (*C*) Forepaw from another E16 *Cd*/*Cd* embryo and +/+ sibling. (*D*) E14 *Cd*/*Cd* exencephalic embryo has a crooked tail with irregular somites including a hemivertebra (arrow on left) a deformed somite (right arrow with asterisk) two small somites (double arrowhead) and deformed somite creating a second bend in the tail (single arrowhead). Asterisks indicate the equivalent somite in +/+ and *Cd*/*Cd* siblings. (*E*) Skeletal defects in an adult *Cd*/*Cd* male that closed the neural tube. Scattered caudal coccygeal (C) and lumbar (L) vertebrae are malformed.

Cd/*Cd* mice were compared with +/+ and the GenBank database.

DNA Constructs. Mouse LRP6 cDNA (J. F. Hess, Merck Research Laboratories) was tagged with a myc-epitope at the C terminus by using a PCR method. LRP6 (G494D) cDNA was made by site-directed mutagenesis (QuikChange, Stratagene). Mouse Dkk-1 cDNA obtained by RT-PCR from embryonic day (E) 10.5 mouse mRNA was epitope FLAG tagged at the C terminus and inserted into expression plasmid pCNA3.1(+). Additional plasmids include the following: FLAG-tagged Mesd (B. C. Holdener, State University of New York at Stony Brook), FLAG-tagged Kremens2 (Krm2) (C. Nierhs, Deutsches Krebsforschungszentrum, Heidelberg), and HA-tagged Wnt1 cDNA (Upstate Biotechnology, Lake Placid, NY).

Wnt Assay in *Cd* Mouse Embryonic Fibroblasts (MEFs) and Transfected NIH 3T3 Cells. MEF cells from E13.5 progeny of mating *Cd*/+ × *Cd*/+ pairs were obtained as described (17). Fetal tissue was used for *Cd* genotyping, later confirmed in cultured fibroblasts. Canonical Wnt signaling was assessed *in vitro* by using the β-catenin stabilization assay (18). Conditioned media (CM) were collected from Wnt3a-secreting mouse L cells and control mouse L cells (American Type Culture Collection) as recommended by American Type Culture Collection. Dkk-1 cDNA was transfected into Cos-1 cells with Lipofectamine 2000, and CM was collected 48 h post-transfection. Unless specified, all antibodies were from Santa Cruz Biotechnology. Secretion of Dkk-1 into media was confirmed by immunoprecipitation (IP)-Western blotting with anti-FLAG antibody (Sigma). CM in the specified dilution was applied to MEF cells or pLrp6-transfected NIH 3T3 cells and incubated for 2 h before protein lysis and Western blot analysis of the cytosolic β-catenin levels (anti-β-catenin, Signal Transduction Laboratory). Optical densities of bands were measured (Quantity One, Bio-Rad) and normalized to anti-extracellular signal-regulated kinase (ERK) labeling of the same blot. Wnt3a or control CM was diluted 1:3 with

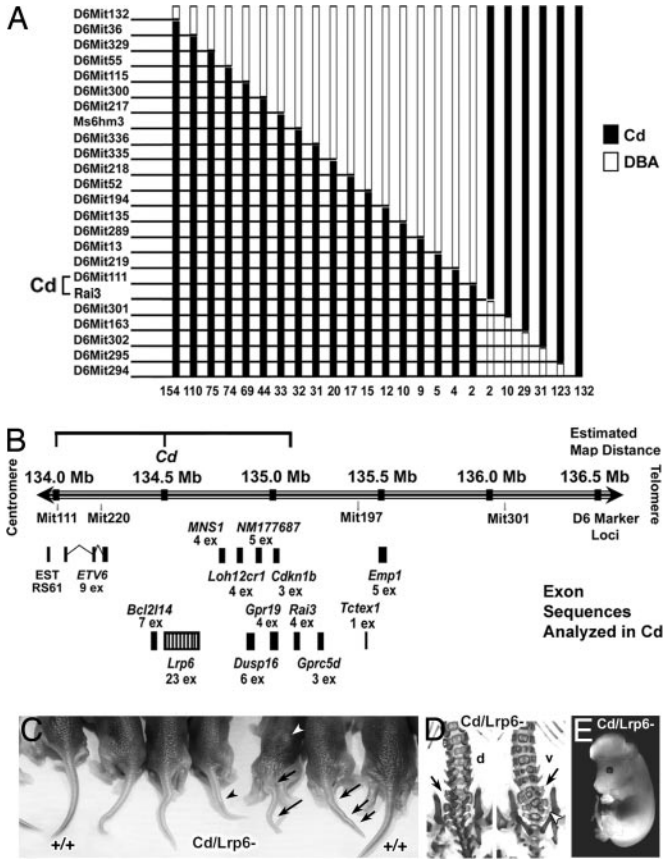

Fig. 2. Genetic and physical maps of the *Cd* locus. (*A*) Polymorphic markers between DBA/2J and *Cd* are shown with a breakpoint between D6Mit111 and *Rai3* (each estimated 0.2 ± 0.14 cM from *Cd*). All 24 markers from D6Mit132 to D6Mit294 had significant LOD scores (logarithm of the likelihood ratio), with a highest score of 299.6 and the lowest 118.1 (Table 1). (*B*) Physical map of the critical *Cd* genomic region shows the relative positions of markers and genes that were sequenced from *Cd* mice. (*C*–*E*) Progeny from *Cd*/+ × *Lrp6*$^{+/-}$ mice reveal the full *Cd*/*Cd* range of phenotypes. In *C*, five double heterozygous *Cd*/*Lrp6*$^{-}$ pups are flanked by +/+ siblings and show mildly (black arrowhead) to severely (arrows) crooked tails. One pup has an irregular spine (white arrowhead) whose skeletal staining (*D*) reveals fused vertebrae (arrow) and a hemi-vertebra (white arrowhead). A *Cd*/*Lrp6*$^{-}$ embryo displays exencephaly (*E*), which, like lumbar vertebral defects, has been seen only in *Cd*/*Cd* mice. d, dorsal; v, ventral. For gene abbreviations, see Table 2.

serum-free medium. For the Dkk-1 inhibition assay, the CM was mixed in the ratio: Wnt3a:serum-free medium:Dkk-1 = 1:2:1. Transfected Lrp6 proteins were biotinylated on the cell surface as described by using 0.5 mg/ml Sulfo-HNS-Biotin and detected in myc-pull-downs by binding of streptavidin-horseradish peroxidase (HRP) conjugate (Pierce) (19).

Results

Exencephaly in *Cd* mice suggested a primary defect in midbrain closure (Fig. 1*A*). Our skeletal stains of multiple *Cd*/*Cd* animals were consistent with the original description of *Cd* 50 years ago in that no instances of frank or occult spina bifida were observed (20). *Cd* was outcrossed in the 1980s to maintain vigor in the line and in the 1990s with 129/SvJ, C57BL/6J, CAST/Ei, and DBA/2J to examine penetrance of the mutation (5), but spina bifida was not observed. Thus, differences in genetic modifiers were not responsible for the lack of spinal NTD in homozygotes. However, *Cd*/*Cd* mice that completed neurulation had severe malformations of caudal vertebrae occurring as high as thoracic level (Fig. 1 *D* and *E*). Limbs and digits were normally formed

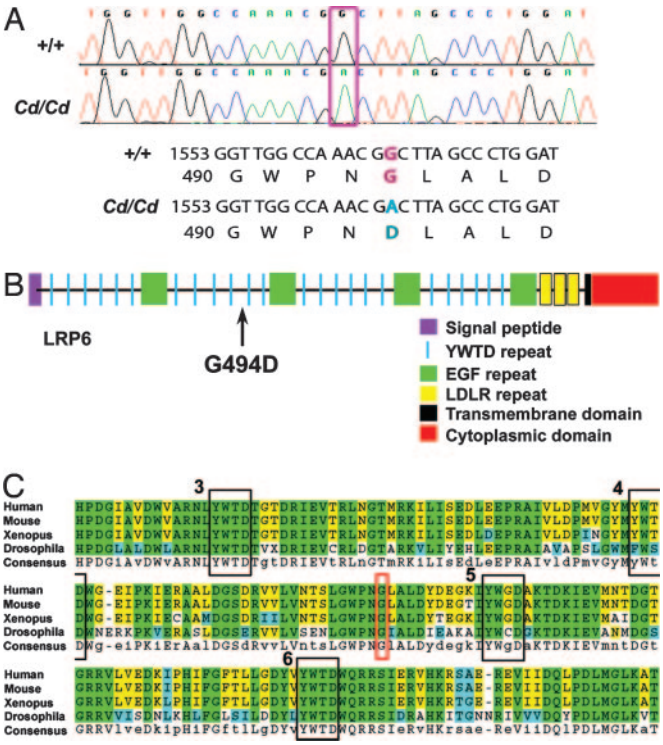

Fig. 3. DNA sequence analysis of the *Lrp6* gene in *Cd*. (*A*) All 23 exons in *Lrp6* were sequenced in *Cd*/*Cd* mice. Compared with +/+ siblings, the mouse database and 9 additional mouse strains, *Cd* differed only in exon 7 with a G1567A substitution that predicts a glycine to aspartate substitution of amino acid 494. (*B*) The LRP6 protein motifs and location of the G494D alteration in the second YWTD-EGF-like repeat (sequence detailed in Fig. 7). (*C*) Species comparison in the second YWTD repeat of LRP6. The mutated glycine residue (red box) is highly conserved. YWTD repeats 3–6 are indicated. Green, identical in 4/4; yellow, 3/4; blue, unique or 2/4.

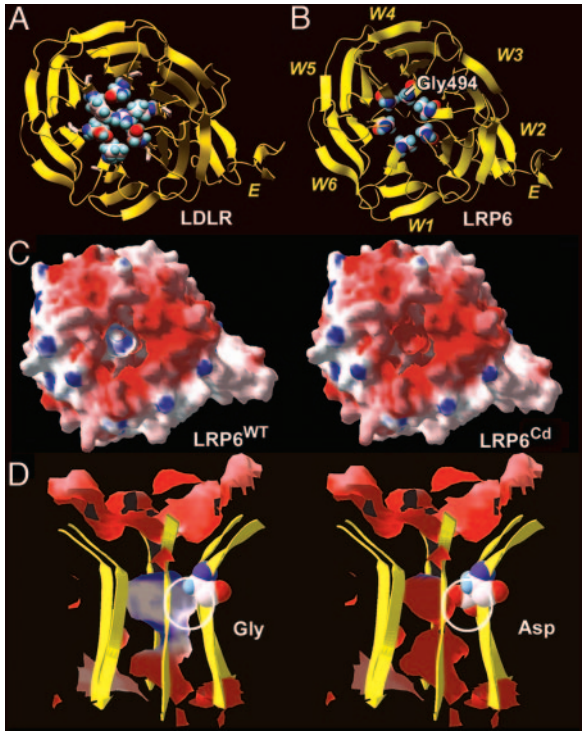

Fig. 4. Molecular modeling of LRP6^{Cd} protein. (*A*) Space filled residues in position X of PXG motifs are shown in the crystal structure of LDLR YWTD-EGF domain (Protein Data Bank ID code 1IJQ). White sticks are prolines N-terminal to them. The X residues pack tightly to cover the gate of the central channel formed by six YWTD repeats. (*B*) The second YWTD-EGF domain in mouse LRP6^{WT} and LRP6^{Cd} based on *A* (sequence alignment in Fig. 7). E, EGF domain; W1–W6, wing or blade of the propeller. (*C*) Top view (same viewing angle as *B*) shows electrostatic potential (E.P.) surfaces of LRP6^{WT} and LRP6^{Cd}. Contributions by X residues in PXG motifs were removed to expose the changes in surface E.P. in the central channel predicted for the *Cd* mutation. (*D*) Cut away side view of the E.P. surfaces forming the channel. Regions of negative surface E.P.s are red (<-15 kT), and of positive potential (>15 kT) are blue. Homology modeling was performed by using MODELLER 4 (35). Panels *A* and *B* were prepared with MOLMOL (36). The E.P.s and molecular surface were calculated by using GRASP (37). The surfaces displayed in *C* and *D* were prepared in SWISS-PDBVIEWER 3.7 (38).

on all strain backgrounds examined (Fig. 1 *A–C*). Illustrated by the alcian blue staining of the E14 *Cd*/*Cd* mouse in Fig. 1*E*, the crooked tail results from deformities of somites/early vertebrae, including hemivertebrae, misshapen or fused vertebrae, and smaller somites with reduced intervertebral spaces. These features are typical of the "Wirbel-Rippen-Syndrom" (WRS), a group of classical mouse mutants to which the Crooked tail strain has been assigned (21). No occurrence of polydactyly/syndactyly were reported in the >2,000 mice examined by Morgan (20) or in >3,000 *Cd* animals phenotyped in our studies. There may be some delay in the secondary ossification sites in the digits (Fig. 1*C*).

For linkage analysis, *Cd*/+ heterozygotes were crossed with DBA/2J to produce an F_1 generation, and 73 crooked tailed F_1 offspring were mated with A/J mice (original background of *Cd*) to obtain N_2 backcross progeny. Because the phenotype is incompletely penetrant, only affected mice are certain to carry the *Cd* mutation. Therefore, normal-tailed F_1 and N_2 mice were excluded from analysis. The 0.2 cM critical interval for *Cd* was further refined by using 24 polymorphic markers on distal chromosome 6 (5). Among 1,043 N_2 offspring, 2 recombinants arose between *Cd* and D6Mit111, 2 recombinants arose between *Cd* and *Rai3*, and 10 recombinants arose between *Cd* and D6Mit301 (Fig. 2*A* and Table 1, which is published as supporting information on the PNAS web site).

A physical map of the *Cd* genomic region is shown in Fig. 2*B*, based on the mouse genome database (15, 16). Sequence analysis found no differences between *Cd*/*Cd* and +/+ in eight of nine candidates in the critical region between D6Mit111 and *Rai3* (Fig. 2*B* and Table 2, which is published as supporting information on the PNAS web site). The high resolution linkage data placed *Cd* within a 1-Mb nonrecombinant region at a position close to *Lrp6* (indicated by the 95% confidence intervals in Table 1). Supporting *Lrp6* as a *Cd* candidate, a gene trap with a full-null mutation of *Lrp6* produced both spinal and cranial NTD as well as limb defects and truncation of the tail (7). Double heterozygous offspring from *Cd*/+ crossed with *Lrp6*$^{+/-}$ mice displayed the full range of *Cd*/*Cd* phenotypes (Fig. 2 *C–E*) including embryonic lethality, indicating that *Cd* and *Lrp6*$^{-}$ are alleles of the same gene. Of the 23 *Lrp6* exons, a single nucleotide substitution was found in exon 7 (Fig. 3) but not in +/+ siblings or an additional nine strains (C57BL/6J, A/He/J, A/J, 129P3/J, BALB/cByJ, CBA/CaJ, DBA/2J, SPRET/Ei, and CAST/Ei), including A/J, a direct descendant of the strain in which *Cd* arose. The mutation replaces a highly conserved glycine with aspartate (G494D) in the second YWTD-EGF repeat domain (Fig. 3).

Computational modeling of LRP6^{Cd} is based on the crystal structure of the LDL receptor (LDLR), in which each YWTD-EGF repeat domain forms a six-bladed β-propeller structure that enables protein–protein interactions (22) (Fig. 4*A*). Comparison of LRP6^{Cd} with the LDLR indicates a packing solution

GENETICS

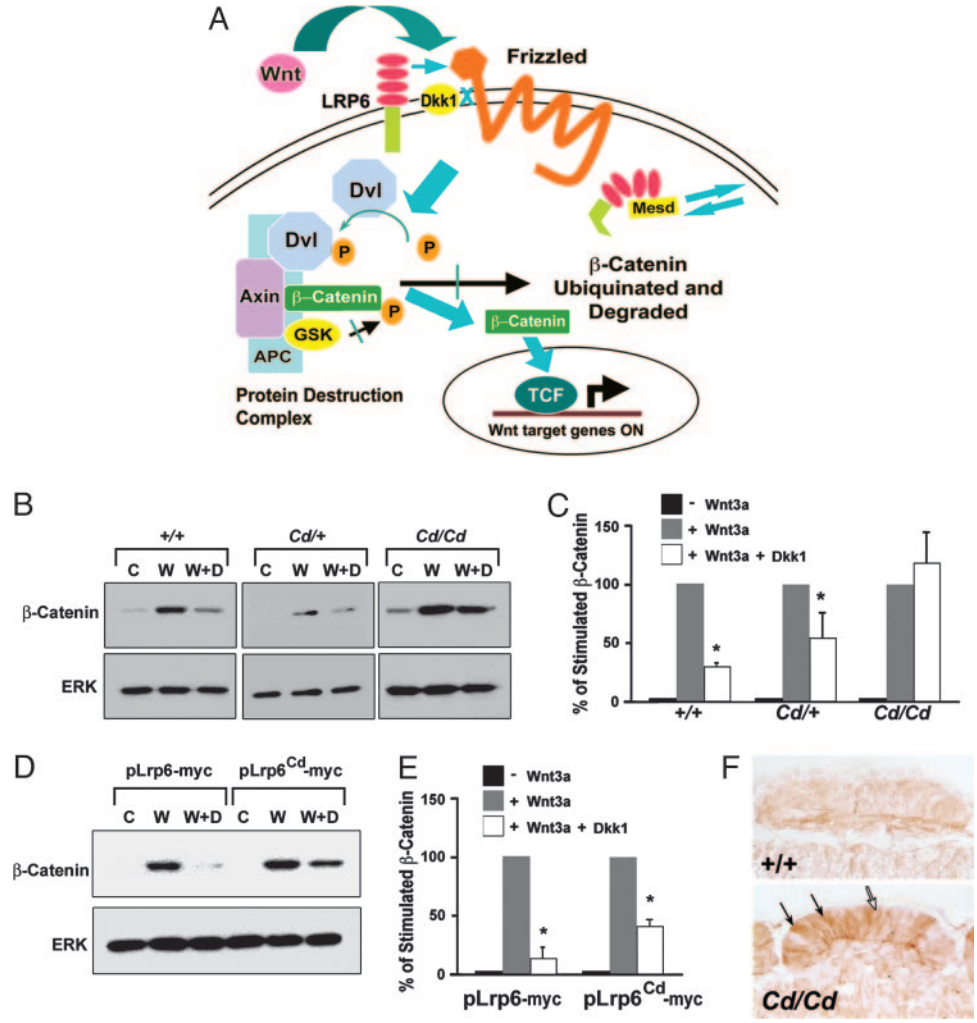

Fig. 5. *Lrp6*^{Cd} and Wnt canonical signaling. (*A*) A multi-protein complex facilitates the glycogen synthase kinase 3β (GSK3β)-mediated phosphorylation of β-catenin for destruction by the E3 ubiquitin ligase complex. Wnt signals through LRP6-Frizzled to activate disheveled (Dvl), which binds axin to inhibit GSK3β phosphorylation of β-catenin, inhibiting ubiquitination and increasing β-catenin levels, which then translocates to activate TCF/LEF [transcription factor (T cell-specific)/lymphoid enhancer-binding factor 1] family transcription factors. Trafficking of Lrp6 into and out of the membrane is facilitated by the chaperone action of Mesd. (*B*) Wnt signaling through β-catenin in MEFs derived from $+/+$, *Cd*/$+$, and *Cd*/*Cd* siblings at E13. Cytosolic β-catenin levels are normalized to total extracellular signal-regulated kinase (ERK) on Western blot analysis. Although Wnt3a CM stimulates canonical signaling, Dkk1 cannot antagonize Wnt3a stimulation in *Cd*/*Cd* cells whereas *Cd*/$+$ MEFs show intermediate response. C, control; W, Wnt3a; D, Dkk1. (*C*) Densitometry of three separate experiments. The levels of stimulated β-catenin in Wnt3a-treated MEF cells were normalized to 100% and compared with cells treated with Wnt3a plus Dkk1 CM. (*D*) Cytosolic β-catenin assays in NIH 3T3 cells after transfection with plasmids expressing myc-tagged WT Lrp6 (pLrp6-myc) or the G494D mutant (pLrp6^{Cd}). (*E*) Quantification of three experiments shows Wnt signaling in pLrp6-myc-transfected cells is reduced 80% by exogenous Dkk1 whereas pLrp6^{Cd}-transfected cells are reduced by only 55%, similar to heterozygous Cd/$+$ MEFs. (*F*) Caudal somites from E9.5 siblings stained with β-catenin antibody (1:100,000 dilution; 6-μm paraffin sections; $\times$60 magnification) show more β-catenin cytosolic (open arrow)/nuclear (filled arrows) labeling in the *Cd*/*Cd* embryo, consistent with Wnt hyperactivity *in vivo*. *, $P < 0.01$.

for the blades (Fig. 4*B* and Fig. 7, which is published as supporting information on the PNAS web site). The G494D mutation resides in a hinge region of blade 4 of the second propeller that brings together a conserved "PXG" motif in which proline (Fig. 4*A*) initiates the β-bend whereas position "X" is an asparagine or another residue with a large volume side chain. Six residues from each blade pack tightly at the gate of the central axis or "channel." The glycine or alanine residue in the PXG (Fig. 7) anchors the position of residue X, and a replacement in this position would disrupt the packing of X at the gate. Comparison of the computed surface electrostatic potentials for the second propeller of LRP6^{WT} with LRP6^{Cd} suggests that the mutation changes the channel properties in the motif in a manner that is likely to affect interactions in a signaling mechanism (Fig. 4 *C* and *D*).

Members of the LDLR family, LRP5 and LRP6, are coreceptors for Fz and are required for Wnt-dependent β-catenin signaling (23). Canonical Wnt signaling (Fig. 5*A*) was therefore examined in *Cd*/*Cd* and WT MEF cells, assessed by the amount of cytosolic β-catenin detected on Western blot analysis. In the presence of Wnt3a, β-catenin levels increased 6- to 10-fold in $+/+$, *Cd*/$+$, and *Cd*/*Cd* MEF cells (Fig. 5 *B* and *C*), indicating that Wnt can signal through LRP6-Fz in *Cd* cells. Several important Wnt modulators interact with LRP6, including its antagonist Dkk1 (24). In these cultures, Dkk1 effectively inhibited Wnt activity in $+/+$ MEFs (WT, reduced by 70%), but could not block Wnt signaling in the *Cd*/*Cd* MEF cells, whereas *Cd*/$+$ MEFs displayed an intermediate response to Dkk1 (Fig. 5*C*). Transfections of $+/+$ and Lrp6-G494D plasmids into NIH 3T3 cells tested whether the point mutation would also impair

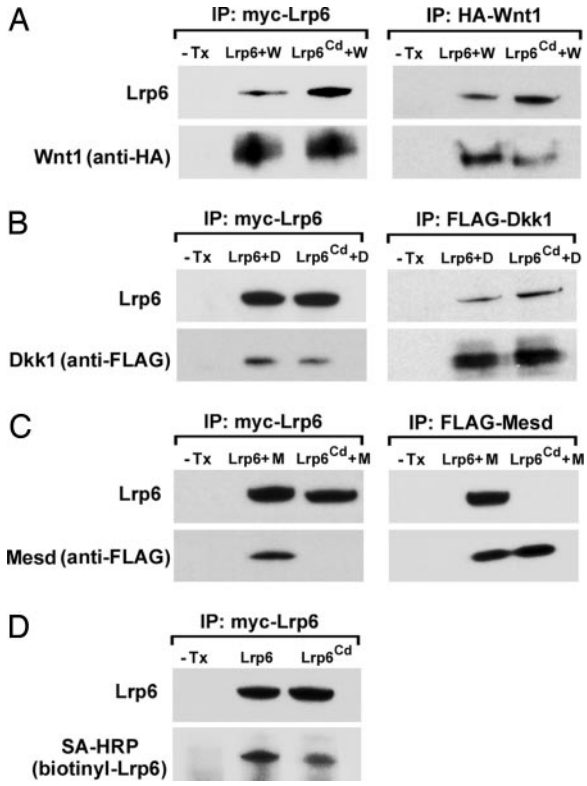

Fig. 6. *Lrp6^{Cd}* retains Wnt and Dkk1 but ablates Mesd binding. Shown are COS cells transfected with pLrp6-myc or pLrp6^{Cd}–myc and one of the following: pDkk1-FLAG (D), pWnt1-HA (W), or Mesd-FLAG (M). Untransfected (-Tx) cultures were controls. (*A*) Lysates were IP'd with anti-myc or anti-HA and run on Western blots developed with anti-Lrp6 or anti-HA antibodies. (*B*) Lysates IP'd with myc or FLAG antibodies pulled down both Lrp6 and Dkk1. (*C*) Lysates IP'd with myc or FLAG antibodies pulled down WT Lrp6 and Mesd but did not co-IP Lrp6^{Cd} and Mesd. (*D*) Cells transfected with myc tagged Lrp6^{wt} or Lrp6^{Cd} were biotinylated on their surfaces. Cell lysates were IP'd with anti-myc, and Western blots were developed with either streptavidin (SA)-conjugated horseradish peroxidase or anti-Lrp6. Equivalent amounts of myc-Lrp6 proteins were present, whereas lower amounts of myc-Lrp6^{Cd} were inserted into the plasma membrane.

Dkk1 on a WT genetic background, far removed from the Cd strain (Fig. 5 *D* and *E*). Indeed, cultures transfected with pLrp6^{Cd}-myc showed impaired Wnt inhibition by Dkk1, similar to the levels seen in *Cd*/+ MEFs. We conclude that, in the presence of mutated LRP6^{Cd}, the Wnt antagonist, Dkk1, does not properly regulate Wnt canonical signaling.

We next examined E9.5 embryos for evidence of Wnt hyperactivity in caudal somites of *Cd*/*Cd* exencephalic embryos compared with WT siblings, using serial dilutions of anti-β-catenin immunostaining (Fig. 5*F* and Fig. 8, which is published as supporting information on the PNAS web site). Genotypes were confirmed by using DNA from embryonic yolk sacks. Greater accumulations of nuclear β-catenin were detected in cells of caudal somites in *Cd*/*Cd* compared with +/+ embryos. These data suggest higher levels of Wnt signaling in *Cd*/*Cd* embryos during neurulation.

Epitope tagged Lrp6, Wnt1, Dkk1, Mesd, or Krm2 were transfected into COS cells to test interactions. Wnt1 was still able to bind to LRP6^{Cd} in a coimmunoprecipitation (co-IP) assay, whether pulling down epitope-tagged Lrp6 or Wnt1 (Fig. 6*A*). Despite the loss of antagonism, Dkk1 bound to Lrp6^{Cd} (Fig. 6*B*) and Krm2, a transmembrane protein that can potentiate Dkk1 inhibition, co-IP'd with Lrp6^{Cd} (Fig. 9, which is published as supporting information on the PNAS web site). Mesd interacts with Lrp5/6 as a chaperone protein that facilitates trafficking of Lrp6 into and out of the cell membrane (25) and is reported to bind to the first YWTD domain of Lrp5. The mutant Lrp6^{Cd} protein did not co-IP with Mesd, whether the pull down targeted Lrp6 (myc) or Mesd (FLAG) (Fig. 6*C*). Transfected myc-Lrp6^{Cd} nevertheless inserted into plasma membrane, although less efficiently (Fig. 6*D*).

Discussion

The *Cd* G494D mutation clearly alters Lrp6 function. First, it replaces a highly species conserved G residue with D, found in *Cd*/*Cd* and not +/+ siblings or nine other mouse strains. Second, molecular modeling of Lrp6 G494D predicts a significant change in its structural properties. Third, the *Lrp6^{Cd}* mutation is shown to interfere with Dkk1 antagonism of Wnt signaling in *Cd*/*Cd*-derived MEFs and in pLrp6^{Cd}-transfected 3T3 cells. That Lrp6^{Cd} results in Wnt hyperactivity is supported by the elevated β-catenin in caudal somites of E9.5 *Cd*/*Cd* embryos compared with +/+ siblings. The causal association between *Lrp6^{Cd}* and *Cd* defects is supported by the fact that Lrp6G494D is the only mutation detected among the coding sequences of 14 genes in the *Cd* region. Moreover, the axial skeletal defects in a different, hypomorphic Lrp6R886W mutation in *ringelschwanz* (*rs*) have been independently ascribed to the same Wirbel-Rippen-Syndrom phenotypic group of mouse mutants as *Cd* (9). Interestingly, whereas the *Lrp6* full-null displays either spina bifida or exencephaly, *rs*/*rs* displays spina bifida and *Cd*/*Cd* displays exencephaly exclusively. Finally, the *Cd*/*Lrp6*$^{-}$ double heterozygous mice display the full *Cd*/*Cd* phenotypic range, so that the *Lrp6*-null allele unmasks the *Cd* effects, providing genetic confirmation that *Cd* is a mutation in *Lrp6*.

That G494D in *Lrp6^{Cd}* alters its capacity to be regulated as the Fz coreceptor is supported by comparison with the crystal structure of the LDLR and by analogy with pathogenic mutations in humans involving a closely related Wnt coreceptor, *LRP5* (22, 26–29). In *LRP5*, missense mutations in β-propellers 2 or 3 are associated with a low-bone-density disorder called osteoporosis-pseudoglioma (OPPG) (26). In another disorder, high bone mass (HBM), LRP5 mutation occurs at the surface of the first propeller module, interfering with DKK1 antagonism of WNT signaling (27, 28). Thus, a missense mutation in LRP6 may be similarly anticipated to have a net activating or inhibitory impact, depending on its position within the YWTD-EGFP, β-propeller structure. The surface electrostatic charge of the central channel within the second β-propeller seems to be altered by the disrupted local packing of "X" residues, which are exposed on the channel surface. The experimental results suggest that this change impairs the ability of LRP6 to regulate Wnt signaling in the presence of Dkk1.

Both Lrp5 G171V and Lrp6^{Cd} mutations produce gain-of-function effects, but neither significantly alters Wnt or Dkk1 binding, whereas both mutations abolish Mesd binding (19). It seems then that the first and second β-propeller domains of Lrp5/6 are required for Dkk1 antagonism and Mesd interaction. Because Krm2 is co-IP'd with Lrp6^{Cd} complexes, the inability of Dkk1 to inhibit Wnt signaling is not explained by loss of Krm2 interaction. Molecular modeling underscores the importance of the β-propeller core for regulation of Lrp5/6 function. Indeed, the changes that robustly interfere with Dkk1 antagonism in Lrp5 mutagenesis studies (E721A and R764A) (19), are located in the PXG motif identified here (Fig. 4) and will produce major changes in the electrostatic properties of the core.

A model for Mesd action with Lrp5 that distinguishes intracellular "autocrine" Wnt signaling from secreted "paracrine" Wnt signaling has been proposed (19), based on cotransfection data. Basal paracrine Wnt signaling through Lrp5G171V was thought to be impaired due to decreased receptor trafficking in

the absence of Mesd binding, whereas autocrine Wnt signaling remained intact. Our experiments in MEFs do not support this model, because basal responses to extracellular Wnt3a were indistinguishable between +/+ and *Cd/Cd* genotypes. Moreover, the lack of interaction with Mesd did not abolish the ability of $Lrp6^{Cd}$ to enter the membrane. Furthermore, $pLrp6^{Cd}$-transfected 3T3 cells displayed stimulation by extracellular Wnt that was equivalent to pLrp6, but impaired responses to exogenously applied Dkk1, demonstrating the effect of this mutation on "paracrine" Wnt and Dkk1 action. The present data suggest a more complicated relationship between Lrp5/6 and Mesd than just protein trafficking that bears further investigation.

Lrp6 is the fourth Wnt gene, and most directly linked with the canonical pathway, to be shown capable of producing NTD in mice, joining *Dvl1*, *Dvl2*, and *Axin* (10, 11). Loss of *Dvl2* produces thoracic spina bifida and cardiac outflow defects whereas *Dvl 1/2* double mutants display craniorachischisis (open neural tube from head to lumbar region) (10). Axin (mutated in the Fused NTD mouse) is antagonized by Dvl, and both can function in canonical (β-catenin) and noncanonical planar cell polarity (PCP) signaling pathways (11, 30–33). The total loss of *Lrp6* produces severe rostral/caudal NTD, limb defects, and tail truncation (7), whereas a hypomorphic allele produces osteoporosis, caudal axial skeletal defects, spina bifida, and "occasional" polysyndactyly (9). In contrast, the $Lrp6^{Cd}$ missense mutation reported here produces functional overexpression (hyperactivity) and associated cranial NTD in addition to caudal vertebral defects. These converging observations implicate Wnt pathways in NTD and suggest that both positive and negative regulation of Wnt signaling is important for neurulation.

Interestingly, Lrp5/6 are most closely associated with canonical Wnt pathways, although attention has recently been drawn to PCP mechanisms in neurulation (34). Three mutations of Lrp6–null (7), hypomorphic (9), and hypermorphic (present report) are now associated with NTD. These mutations suggest that both Wnt-associated PCP and canonical pathways contribute to neurulation. Alternatively, the view that Lrp5/6 participate exclusively in canonical pathways may have to be reevaluated. Moreover, the $Lrp6^{Cd}$ mutation suggests that even a subtle change in the LRP6 sequence can result in significant birth defects that are ameliorated by folate, despite the fact that the affected gene itself is not a direct participant in folate transport or metabolism.

We thank Drs. B. C. Holdener, J. F. Hess, and C. Nierhs for their generous gifts of pMesd, Lrp6 cDNA, and pKrm2; Dr. Anthony Brown for helpful discussion of the Wnt assay; and Tom Iadecola for photography. This work was supported by National Institute of Neurological Disorders and Stroke Grant RO1 NS24998 (to M.E.R.).

1. Northrup, H. & Volcik, K. A. (2000) *Curr. Probl. Pediatr.* **30,** 313–332.
2. Seller, M. J. (1981) *J. Med. Genet.* **18,** 245–248.
3. Wald, N., Sneddon, J., Densem, J., Frost, C., Stone, R. & MRC Vitamin Study Research Group (1991) *Lancet* **338,** 131–137.
4. Czeizel, A. E. (2000) *Paediatr. Drugs* **2,** 437–449.
5. Carter, M., Ulrich, S., Oofuji, Y., Williams, D. A. & Ross, M. E. (1999) *Hum. Mol. Genet.* **8,** 2199–2204.
6. Brown, S. D., Twells, R. C., Hey, P. J., Cox, R. D., Levy, E. R., Soderman, A. R., Metzker, M. L., Caskey, C. T., Todd, J. A. & Hess, J. F. (1998) *Biochem. Biophys. Res. Commun.* **248,** 879–888.
7. Pinson, K. I., Brennan, J., Monkley, S., Avery, B. J. & Skarnes, W. C. (2000) *Nature* **407,** 535–538.
8. Schweizer, L. & Varmus, H. (2003) *BMC Cell Biol.* **4,** 4.
9. Kokubu, C., Heinzmann, U., Kokubu, T., Sakai, N., Kubota, T., Kawai, M., Wahl, M. B., Galceran, J., Grosschedl, R., Ozono, K., *et al.* (2004) *Development (Cambridge, U.K.)* **131,** 5469–5480.
10. Hamblet, N. S., Lijam, N., Ruiz-Lozano, P., Wang, J., Yang, Y., Luo, Z., Mei, L., Chien, K. R., Sussman, D. J. & Wynshaw-Boris, A. (2002) *Development (Cambridge, U.K.)* **129,** 5827–5838.
11. Zeng, L., Fagotto, F., Zhang, T., Hsu, W., Vasicek, T. J., Perry, W. L., 3rd, Lee, J. J., Tilghman, S. M., Gumbiner, B. M. & Costantini, F. (1997) *Cell* **90,** 181–192.
12. Parr, B. A. & McMahon, A. P. (1995) *Nature* **374,** 350–353.
13. Suzuki, S., Mitani, K., Kuwabara, K., Takahashi, Y., Niwa, O. & Kominami, R. (1993) *J. Biochem.* **114,** 292–296.
14. Manly, K. F. (1993) *Mamm. Genome* **4,** 303–313.
15. Eppig, J. T., Bult, C. J., Kadin, J. A., Richardson, J. E., Blake, J. A., Anagnostopoulos, A., Baldarelli, R. M., Baya, M., Beal, J. S., Bello, S. M., *et al.* (2005) *Nucleic Acids Res.* **33,** D471–D475.
16. Hubbard, T., Andrews, D., Caccamo, M., Cameron, G., Chen, Y., Clamp, M., Clarke, L., Coates, G., Cox, T., Cunningham, F., *et al.* (2005) *Nucleic Acids Res.* **33,** D447–53.
17. Serrano, M., Lin, A. W., McCurrach, M. E., Beach, D. & Lowe, S. W. (1997) *Cell* **88,** 593–602.
18. Willert, K., Brown, J. D., Danenberg, E., Duncan, A. W., Weissman, I. L., Reya, T., Yates, J. R., 3rd & Nusse, R. (2003) *Nature* **423,** 448–452.
19. Zhang, Y., Wang, Y., Li, X., Zhang, J., Mao, J., Li, Z., Zheng, J., Li, L., Harris, S. & Wu, D. (2004) *Mol. Cell. Biol.* **24,** 4677–4684.
20. Morgan, W. (1954) *J. Gene.* **52,** 354–373.
21. Theiler, K. (1988) *Adv. Anat. Embryol. Cell Biol.* **112,** 1–99.
22. Jeon, H., Meng, W., Takagi, J., Eck, M. J., Springer, T. A. & Blacklow, S. C. (2001) *Nat. Struct. Biol* **8,** 499–504.
23. He, X., Semenov, M., Tamai, K. & Zeng, X. (2004) *Development (Cambridge, U.K.)* **131,** 1663–1677.
24. Mao, B., Wu, W., Li, Y., Hoppe, D., Stannek, P., Glinka, A. & Niehrs, C. (2001) *Nature* **411,** 321–325.
25. Hsieh, J. C., Lee, L., Zhang, L., Wefer, S., Brown, K., DeRossi, C., Wines, M. E., Rosenquist, T. & Holdener, B. C. (2003) *Cell* **112,** 355–367.
26. Gong, Y., Slee, R. B., Fukai, N., Rawadi, G., Roman-Roman, S., Reginato, A. M., Wang, H., Cundy, T., Glorieux, F. H., Lev, D., *et al.* (2001) *Cell* **107,** 513–523.
27. Little, R. D., Carulli, J. P., Del Mastro, R. G., Dupuis, J., Osborne, M., Folz, C., Manning, S. P., Swain, P. M., Zhao, S. C., Eustace, B., *et al.* (2002) *Am. J. Hum. Genet.* **70,** 11–19.
28. Boyden, L. M., Mao, J., Belsky, J., Mitzner, L., Farhi, A., Mitnick, M. A., Wu, D., Insogna, K. & Lifton, R. P. (2002) *N. Engl. J. Med.* **346,** 1513–1521.
29. Van Wesenbeeck, L., Cleiren, E., Gram, J., Beals, R. K., Benichou, O., Scopelliti, D., Key, L., Renton, T., Bartels, C., Gong, Y., *et al.* (2003) *Am. J. Hum. Genet.* **72,** 763–771.
30. Zhang, Y., Qiu, W. J., Chan, S. C., Han, J., He, X. & Lin, S. C. (2002) *J. Biol. Chem.* **277,** 17706–17712.
31. Miller, J. R., Hocking, A. M., Brown, J. D. & Moon, R. T. (1999) *Oncogene* **18,** 7860–7872.
32. Wallingford, J. B., Fraser, S. E. & Harland, R. M. (2002) *Dev. Cell* **2,** 695–706.
33. Gong, Y., Mo, C. & Fraser, S. E. (2004) *Nature* **430,** 689–693.
34. Copp, A. J., Greene, N. D. & Murdoch, J. N. (2003) *Nat. Rev. Genet.* **4,** 784–793.
35. Sali, A. & Blundell, T. L. (1993) *J. Mol. Biol.* **234,** 779–815.
36. Koradi, R., Billeter, M. & Wuthrich, K. (1996) *J. Mol. Graphics* **14,** 51–55, 29–32.
37. Nicholls, A., Sharp, K. A. & Honig, B. (1991) *Proteins* **11,** 281–296.
38. Guex, N. & Peitsch, M. C. (1997) *Electrophoresis* **18,** 2714–2723.